crystals

MDPI

Article

Simulation and Experimental Analysis of Tool Wear and Surface Roughness in Laser Assisted Machining of Titanium Alloy

Xianjun Kong *, Zhanpeng Dang, Xiaole Liu, Minghai Wang and Ning Hou

School of Mechatronics Engineering, Shenyang Aerospace University, Shenyang 110136, China
* Correspondence: kongxianjun.2008@163.com

Abstract: A three-dimensional cutting simulation prediction model based on DEFORM-3D finite element software was developed and experimentally validated, with a maximum error of 21.1% between the experimental and simulation results. The effects of the difference in cutting mechanism between conventional machining (CM) and laser-assisted machining (LAM) of TC6 titanium alloy on the tool wear and the surface roughness were investigated in terms of the cutting force and the cutting temperature. The depth of the laser-heated layer was mainly responsible for the difference in the cutting mechanism between the two methods. When the depth of the heating layer was smaller than the cutting depth, the tool wear of the LAM was larger than that of the CM. When the depth of the heating layer was larger than the cut depth, the surface roughness of the LAM was higher than that of the CM. Range analysis revealed that the cutting speed had the largest effect on the maximum wear depth of the rake face. Based on linear regression analysis, the cutting depth had a larger effect on the surface roughness in LAM. The average error between the linear regression prediction equation and the experimental results for surface roughness was 4.30%.

Keywords: DEFORM-3D; LAM; TC6 titanium alloy; tool wear; surface roughness

Citation: Kong, X.; Dang, Z.; Liu, X.; Wang, M.; Hou, N. Simulation and Experimental Analysis of Tool Wear and Surface Roughness in Laser Assisted Machining of Titanium Alloy. *Crystals* **2023**, *13*, 40. https://doi.org/10.3390/cryst13010040

Academic Editor: Jiandong Wang

Received: 24 November 2022
Revised: 21 December 2022
Accepted: 22 December 2022
Published: 26 December 2022

1. Introduction

Titanium alloys have high specific strength as well as good heat and corrosion resistance, and they are widely used in aerospace, weaponry and automobile manufacturing, including the manufacturing of aircraft structural components, missile shells, light artillery components and automobile engine connecting rods. However, owing to the poor thermal conductivities and solid chemical activities of titanium alloys, they cause the cutting process to involve excessive cutting forces, high cutting temperatures and severe tool wear problems, which adversely affect the surface quality of the processed workpiece, thereby increasing production costs and decreasing production efficiency [1,2].

Haoqian et al. [3] used ABAQUS software to simulate and analyse the cutting of the TC4 material and found that the rake angle of the tool significantly influenced the cutting force and that the cutting power increased significantly when the rake angle was negative. Yuyan et al. [4] performed dry milling of titanium alloy Ti–6Al–4V with YG6 carbide tools and found that the tool wear increased with the increasing cutting speed. Zhangyong et al. [5] studied the effect of cutting parameters on the cutting force of the turned titanium alloy by developing a simulation model of the turned titanium alloy. It was found that cutting speed was inversely proportional to the cutting force, and the feed was positively proportional to the cutting force and had a greater impact on the cutting force. Zhenghuan et al. [6] proposed a method for predicting the cutting force during milling of titanium alloy in a manufacturing equipment based on a multilayer fusion network structure.

In addition to conventional machining (CM), several new methods have recently been developed for difficult-to-machine materials, such as laser-assisted machining (LAM). LAM is a complex machining technique that employs a laser to modify the properties of a material being machined, reducing cutting forces, minimising the tool wear, as well as enhancing the tool life, productivity and surface quality [7].

Based on experimental and simulation results on conventional and ultrasonic vibration-assisted turning processes in Ti−6Al−4V titanium alloys, Rudranarayana et al. [8] investigated the effect of process parameters on the force. It was found that there is a significant reduction of the cutting force during the ultrasonic vibration-assisted turn due to the intermittent effect of the cutting insertion. In addition, the cutting force during the ultrasonic vibration-assisted turning process increases with the velocity due to the increased contact time of the cutting with the workpiece insertions.

Wu et al. [9] used laser cutting technology to study the microstructure and properties of the heat-affected zone of TA15 titanium alloy. The results showed that the thermally affected region consisted of melting and non-melting regions, and the grain size gradually increased from the non-melting region to the melting region. The microscopic hardness decreased from the heat-affected zone to the matrix, and the yield and the tensile strength of the sheets in the heat-affected zone were lower than those in the non-heat-affected zone.

Turnad et al. [10] studied the effects of thermal-assisted machining on the suppression of vibrations during the end milling of titanium alloys Ti−6Al−4V using PCD inserts. Induction coil heating was utilised to generate heat close to the cutting zone prior to cutting. It was observed that increasing the preheating temperature results in reductions of the chip shrinkage coefficient and the primary chip serration frequency. The suppression of vibration/chatter was exposed as another benefit of applying high-frequency induction heating to the end milling of the titanium alloy Ti−6Al−4V.

Habrat from Poland carried out LAM experiments on Ti–6Al–4V alloy with carbide cutting tools and found that the tangential component of the cutting force could be reduced by more than 60% when appropriate cutting parameters were selected [11].

In Korea, Woo et al. performed laser-assisted milling on the surface of a TC4 titanium alloy after directional deposition. A real-time laser control system was used to preheat the material during laser-assisted milling. The results showed that the cutting force and the surface roughness were reduced by >40% and >30%, respectively [12].

Gao et al. [13] conducted an experimental study on the laser-assisted milling of titanium alloy TC4. They found that the cutting force and the tool wear rate were significantly reduced.

Kalantari et al. [14] investigated the surface integrity characteristics of Ti6−Al−4V alloy when machined using conventional and LAM processes. Further, the surface integrity and heat load generated during the material removal process were evaluated under different machining parameters.

Ayed and Germain [15] performed simulations using ABAQUS finite element analysis and experimental investigation and determined that the shear angle and the chip thickness of the turned titanium alloy using LAM decreased as the laser power increased, while the temperature rise of the tool was insignificantly affected by the laser power. Kim et al. [16] presented an experimental investigation on the machinability of titanium alloy Ti–6Al–4V using laser-assisted end milling process. Their results proved that heat assistance significantly influenced the magnitude of the cutting forces, while the actual reduction in forces varied slightly, depending on the force component, the cutting tool and cutting conditions; the force components showed a 13%–46% reduction. Dandekar et al. [17] performed an experimental study on the LAM of a titanium alloy TC4. The optimal laser heating temperature was set at approximately 250 °C, and a Ti–Al–N-coated carbide cutting tool was used for machining. When compared to conventional machining, the cutting speed was increased to 200 m/min, and the tool life was increased by a factor of two to three. The cutting force was significantly reduced, the machined surface quality was excellent, and ~40% of machining costs were saved.

In summary, LAM offers significant advantages in terms of the reduced cutting force and tool wear. Most of the current research on LAM of titanium alloys has focused on the effect of the cutting parameters on the cutting force, with little attention paid to the mechanisms underlying the difference in surface roughness and tool wear between CM and LAM. Theoretical studies of LAM of TC6 titanium alloys are still imperfect and do not provide a theoretical reference for industrial applications of LAM of titanium alloys. Therefore, by combining the DEFORM software with the orthogonal array/Taguchi method, we improved the cutting mechanism of LAM in terms of the tool wear and the surface roughness and performed a comparative analysis with CM. Finally, the process parameters of LAM of TC6 titanium alloy were optimised, and the surface roughness was predicted and verified.

2. Materials and Methods

2.1. Experimental Set-Up for Turning Experiments

The components of the laser-assisted turning experimental system are shown in Figure 1a. The system comprised four subsystems: cutting, laser heating, cutting temperature measurement and cutting force measurement. It mainly consisted of a CAK4085nj computerised numerical control machine, a 2000W YAG continuous laser head with a wavelength of 1064 nm, a six-axis robot arm, a FLIR T630sc thermal imager and a cutting force measurement system composed of a Swiss Kistler dynamometer and Dynoware software [18]. A physical view of the experimental system is shown in Figure 1b.

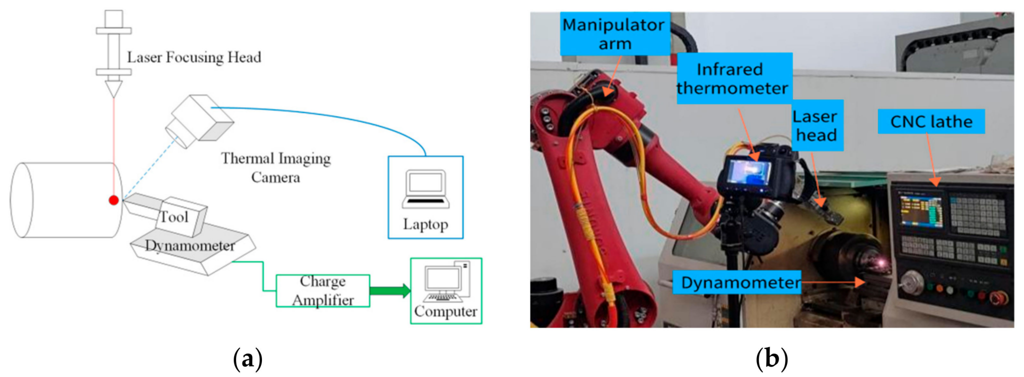

Figure 1. Laser-assisted turning system: (**a**) schematic of the system components; (**b**) physical view of the system.

2.2. Experimental Programme

In the LAM process, the material removal temperature, i.e., the average temperature of the shear zone [19], plays a decisive role in the cutting mechanism, tool wear and machined surface quality. A very low temperature cannot accurately reflect the role of heat-assisted machining, while a very high temperature damages the microstructure of the material matrix and even increases the tool wear.

To maximise the laser absorption rate and focus on the upper surface of the workpiece, a robotic arm was used to precisely adjust parameters such as the direction of laser incidence, the spot size and the distance between the laser spot and the tool by making the angle of incidence equal to the Brewster angle (i.e., the incident light is perpendicular to the reflected light). In addition, because the surface of the workpiece was smooth, the specular reflection phenomenon was evident, and the absorption of laser energy by the material was low. Therefore, the surface of the workpiece was coated with a layer of black ink to increase the absorption of the laser by the workpiece.

During the laser heating process, a FLIR type infrared camera was used to instantly monitor the temperature at the cutting point to ensure that the laser reached the optimal temperature for cutting the TC6 titanium alloy during actual machining. The workpiece was mounted on a three-jaw chuck, and the lathe tool holder was adjusted so that the tip of the tool coincided with the horizontal plane of the workpiece axis, and the tool started its feeding motion 0.2 mm from the front of the workpiece. During the cutting process, the workpiece was mounted on a three-jaw chuck, and a Kistler dynamometer was attached to the lathe's tool holder to record the cutting forces. The Kistler force gauge amplified the collected force signals and outputted the three-way cutting force values. There are several methods for measuring the surface roughness of a workpiece, including the comparative method, the light cutting method, the interferometric method and the stylus method. In this study, the surface roughness of the workpiece after processing was measured using the contact method, and the portable surface roughness tester TIME 3200 was used to measure a point every 120° in the radial direction of the workpiece surface and a point every 3 mm in the axial direction. A total of 9 points were measured. During the measurement, the effects of measurement uncertainty and noise on measurement accuracy were neglected, and the results were averaged.

To investigate how different cutting parameters affected the cutting force, the tool wear and the surface roughness, an orthogonal array was designed. The test was conducted using the standard field method and three factors (cutting speed, depth of cutting and feed). Zheng [20] conducted a study on laser assisted micro-milling of TC4 titanium alloy and found that when the surface temperature of the workpiece was heated by laser at 400 °C, the cutting stress was reduced to about 70% of that in micro-milling. Therefore, the laser-assisted turning of the titanium alloy ensured that the surface of the workpiece was heated to ~400 °C before cutting. The turned workpiece was a cylindrical bar of a 31mm diameter and a 110 mm length, and its material properties are listed in Table 1. The dry-cutting method was used in the experiments. The cut-off length for a single experiment was 10 mm. The laser spot was positioned in front of the cutting tool and moved at the same speed as the tool.

Table 1. TC6 titanium alloy properties.

Grade	Room-Temperature Mechanical Properties (the Minimum Values)				High-Temperature Performance	
					400 °C	
	Tensile Strength Rm (MPa)	Specified Non-Proportional Elongation Strength Rp0.2 (MPa)	Elongation at Break A (%)	Section Shrinkage Z (%)	Rm (MPa)	σ100h (MPa)
TC6	980	840	10	25	735	665

3. Results and Discussion

3.1. Simulation Analysis

3.1.1. Process Simulation Using DEFORM

DEFORM-3D was used to simulate the external turning of the workpiece, with the workpiece set as a plastic body and obeying the von Mises criterion. DEFORM-3D is a powerful process simulation system designed to analyse the three-dimensional (3D) flow of complex metal forming processes. The workpiece material was modelled using the Johnson-Cook (J-C) intrinsic model [21]:

$$\sigma = (A + B\varepsilon^n)[1 + C\ln(\frac{\dot{\varepsilon}}{\dot{\varepsilon}_0})][1 - (\frac{T - T_r}{T_m - T_r})^m], \tag{1}$$

where σ is the yield limit, ε is the equivalent plastic strain, $\dot{\varepsilon}$ is the equivalent plastic strain rate, $\dot{\varepsilon}_0$ is the initial strain rate, A is the initial yield stress of the material, B is the hardening coefficient, C is the strain rate coefficient, m is the temperature softening coefficient, n is the work hardening coefficient, T is the deformation temperature, Tr is the room temperature (20 °C), and Tm is the melting point of the material [21].

The tool wear was used in the Usui model, where friction is an important factor in the cutting process, and the following frictional bond-slip model was used [22]:

$$\omega = \int apve^{-b/T}dt, \tag{2}$$

$$\tau_f(x) = \tau_p;\ \sigma_n(x) \geq \tau_p(0 < x < l_p), \tag{3}$$

$$\tau_f(x) = \mu\sigma_n(x);\ \mu\sigma_n(x) < \tau_p(l_p < x < l_c), \tag{4}$$

where τ_f is the frictional shear stress, σ_n is the positive stress, τ_p is the shear strength, μ is the coefficient of friction, ω is the wear depth, dt is the change in time, p is the interface pressure, v is the sliding speed, T is the absolute interface temperature, a and b are test correction factors, and a and b are 0.0000001 and 855.0, respectively [22].

Figure 2 shows the meshing of the tool and the workpiece on a tetrahedral grid. The smaller mesh size of the tool tip part was 0.1 mm, and the mesh size of the other parts and the workpiece was 0.3 mm. The mesh was a tetrahedral mesh. Table 2 lists the model data. During laser-assisted turning, the workpiece temperature was set to 400 °C to replace the laser heating.

Table 2. Model data.

Type of Generated Element	Tetrahedral Element
Tool/workpiece mesh number (pieces)	20,000/30,000
Form of the workpiece	Body of plasticity
Ambient temperature (°C)	20
CM/LAM workpiece temperature (°C)	20/400

The simulation model used the wear depth of a rake face as the orthogonal test index, and the cutting force was used to verify the accuracy of the simulation. In addition, v, f and ap were used as the test factors, and three levels were set for each factor to obtain a total of nine sets of orthogonal experiments. Three levels and three factors were selected based on the material properties of TC6 titanium alloy and its practical engineering applications, as shown in Table 3; Table 4 lists the specific cutting parameters.

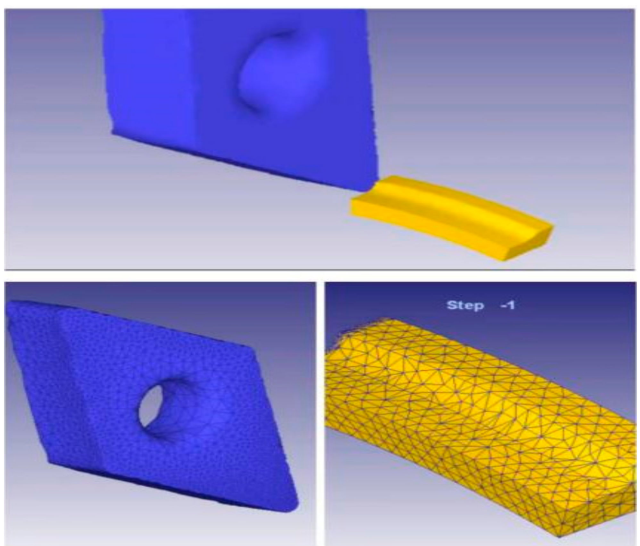

Figure 2. Turning geometry.

Table 3. Orthogonal factor levels.

Level Factors	Cutting Speed v_c (m/min)	Cutting Depth a_p (mm)	Feeding Speed f (mm/r)
Level 1	30	0.1	0.1
Level 2	50	0.3	0.15
Level 3	70	0.5	0.2

Table 4. Experimental layout using an L9 orthogonal array.

Test Group Number	Cutting Speed v_c (m/min)	Cutting Depth a_p (mm)	Feeding Speed f (mm/r)
001	70	0.5	0.2
002	50	0.5	0.1
003	30	0.5	0.15
004	70	0.3	0.1
005	50	0.3	0.15
006	30	0.3	0.2
007	70	0.1	0.15
008	50	0.1	0.2
009	30	0.1	0.1

3.1.2. Simulation Model for the Temperature Field

In laser-assisted turning, the laser heating temperature is critical in determining the optimal result. The scanning speed of the laser increases as the cutting speed increases, and the heating temperature of the laser decreases with the cutting speed. Therefore, when the cutting speed decreases, the laser heating effect increases and the material softens significantly [23]. Evidently, the depth of the softening layer of laser heating is crucial for LAM; therefore, COMSOL simulation software was used to simulate the temperature field of the heating depth of laser scanning of the TC6 titanium alloy. Further, the depth of the heat reaching 400 °C within the material was measured at the same laser power and scanning speeds of 30, 50 and 70 m/min separately. The model was a 10 mm × 1 mm × 1 mm cuboid with 23,460 domain cells, 3206 boundary cells and 278 edge cells.

The surface heat source model can be used for laser heating of the metal surface, and the heat flux distribution can be described by the Gaussian distribution function [24]:

$$Q = \frac{3\alpha P}{\pi r_0^2} \exp(-3\frac{r^2}{r_0^2}), \tag{5}$$

where Q is the surface heat flux of the laser irradiation region, r_0 is the radius of the laser spot, α is the absorption rate of laser energy by the heated material, P is the laser power, and r is the distance from a point to the centre of the laser spot. Considering the extremely short laser heating time and extremely high energy, convection and radiative heat transfer at the surface and outside of the workpiece were neglected, and only heat conduction inside the workpiece was considered. The thermal conductivity and specific heat capacity of TC6 were set to scale with the temperature. The laser absorption rate was measured to be 0.8 using a combination of thermocouples and COMSOL simulations.

3.1.3. Cutting Forces Simulation Validation

Cutting forces are an important physical phenomenon in the metal cutting process. They not only deform the metal in the cutting layer, consume power and generate cutting heat, but they also dull the tool and reduce its cutting power, resulting in poor machining quality. Figure 3 compares the cutting forces obtained from the simulation using DEFORM with the experimentally measured cutting forces, revealing that both conventional machining and LAM did not differ much from the results obtained from the simulation.

The most significant error in CM occurred in the ninth group, with an error rate of 20%, while the most significant error in LAM occurred in the second group, with an error rate of 21.1%, which may be caused by the higher actual cutting temperature than the simulation temperature set, as well as the vibration of the machine tool spindle and the measurement error of the cutting force measurement system during actual machining. Figure 4 shows that the cutting force curve trends of the simulation and the experiment were similar, with a small difference between the two peaks. Therefore, a comparison of simulation and experimental data showed that the 3D turning model developed in this study is accurate.

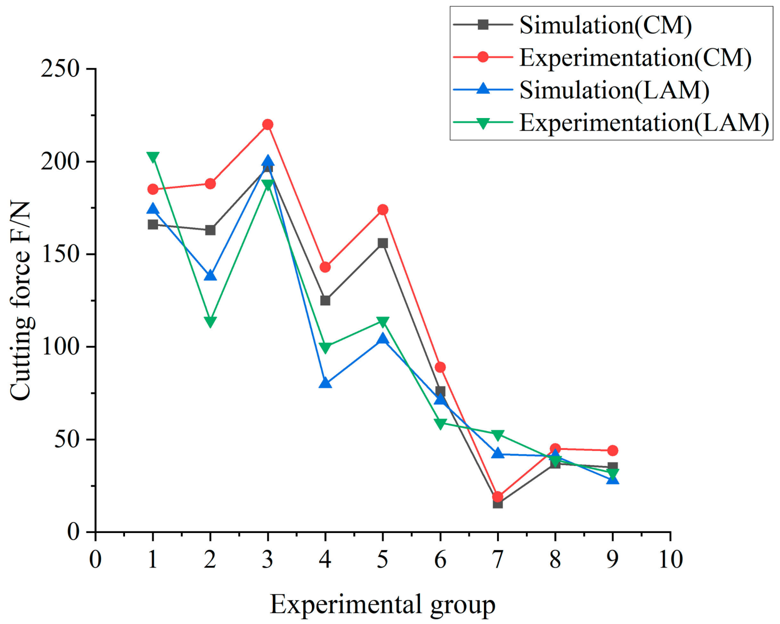

Figure 3. Comparison of simulated and experimental cutting forces.

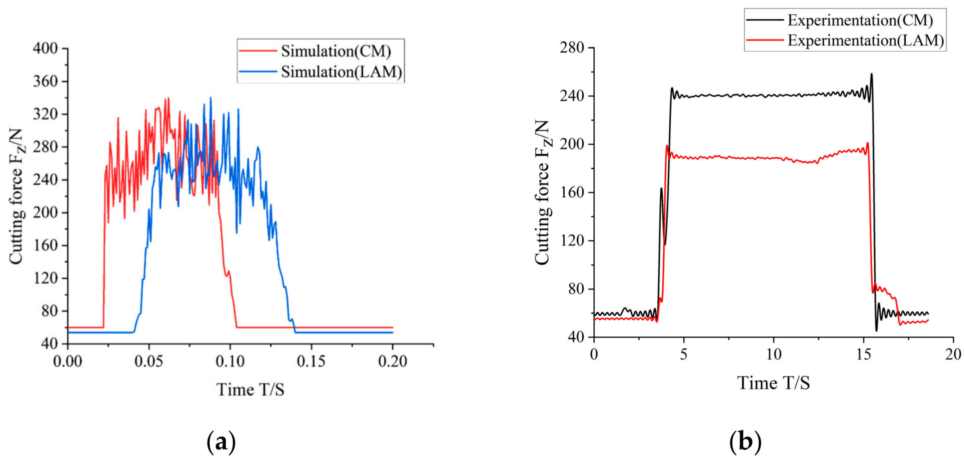

Figure 4. Comparison of simulated and experimental cutting forces curves: (**a**) simulation; (**b**) experimentation.

3.2. Analysis of the Tool Wear

During the cutting process, TC6 titanium alloy is susceptible to forming a hard and brittle surface layer with nitrogen and oxidation from air. As a result, the tool wear is severe, according to a previous study [25]. In general, the tool wear is classified as the wear of the rake face of the cutter and the flank face and the boundary of the tool. The wear of the rake face of the cutter is expressed as the maximum depth of the crater wear KT, and the wear of the rear tool face is expressed as the average wear width VB or the maximum wear width VBmax. When the wear reaches a certain level, the cutting force increases rapidly, the cutting temperature rises sharply and vibration is generated, causing a decrease in the machining accuracy of the workpiece and deterioration in its surface quality. By analysing the wear characteristics of the tool during laser-assisted milling of TC4 titanium alloy, Yanfeng et al. found that laser-assisted milling can reduce the maximum wear on the rear tool face compared to conventional milling but does not improve the average wear on the rear tool face [13]. Therefore, the tool wear was measured using KT on the rake face of the cutter and VBmax on the flank face of the tool.

Figure 5 shows that during CM, severe crescent wear occurred on the rake face of the tool, along with some boundary wear and a micro broken edge. From the DEFORM-3D simulation, the maximum wear depth on the rake face of the cutter from the CM and LAM is presented in Table 5. Evidently, in addition to groups 1, 4 and 7, the wear depth on the rake face of the cutter from the LAM was less than that from the CM. The reduction occurred more in groups 3, 6 and 9, which showed that the cutting speed had the most significant influence.

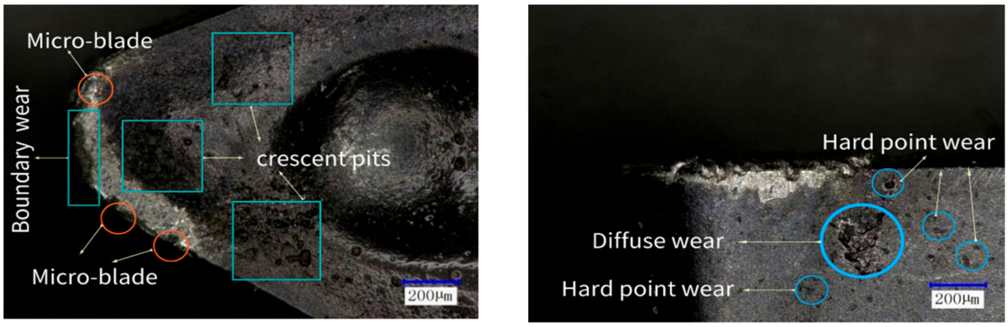

(**a**) (**b**)

Figure 5. Tool wear morphologies in conventional machining (v_c = 50m/min, f = 0.10 mm/rev and ap = 0.5 mm): (**a**) wear morphology on the rake face; (**b**) wear morphology on the flank face.

In addition, the cloud diagram obtained from the simulation (Figure 6) revealed that not only the wear depth of the conventional cutting rake face of the cutter was greater than that of laser-assisted cutting, but the wear range of the conventional cutting rake face of the cutter was greater than that of LAM. The wear depths of the rake face of the cutter of LAM and CM and extreme difference analysis are shown in Table 6. Moreover, Table 6 lists a cutting speed extreme difference of 26.58%, a cutting feed extreme difference of 11.43% and a depth of the extreme cutting difference of 3.01%, which showed that the influencing factors of the tool wear depth are as follows: cutting speed v_c > feeding speed f > depth of cutting ap. Extreme difference analysis was used to determine the optimal combination of cutting parameters for LAM: The cutting parameters were v_c = 30 m/min, f = 0.15 mm/r and ap = 0.5 mm.

The wear depth of the rake face of the cutter from LAM was greater than that from CM, because the cutting speed was faster. Moreover, the material heat transfer was not timely, and the material softening was not apparent, resulting in a minor decrease in the yield strength of the material. However, due to the effect of laser irradiation, the hardness of the material surface increased coupled with the amount of thermal expansion, resulting in the workpiece being processed under the action of the cutting force to produce more significant plastic deformation. Moreover, the chip deformation was more significant in the flow through the extrusion friction of the rake face of the cutter. Therefore, the tool in the cutting process produced sufficient pressure and higher temperature, so that the rake face of the cutter of the tool and the chip experienced serious cold welding.

At the same time, the C and Co in the tool diffused into the chip during high-temperature cutting and were carried away, reducing not only the tool hardness but also the carbide and the bond strength of the substrate. Thus, the rupture of the bond point of bond occurred on the tool side, and the bond wear on the rake face of the cutter was more severe, ultimately leading to a slightly higher tool wear depth by LAM than that of the CM. In LAM of single-crystal silicon, Liu et al. [26] discovered that the tool wear could only be reduced at the optimal heating temperature. Further, in laser-assisted turning, the appropriate laser heating temperature is the key to determining the effectiveness.

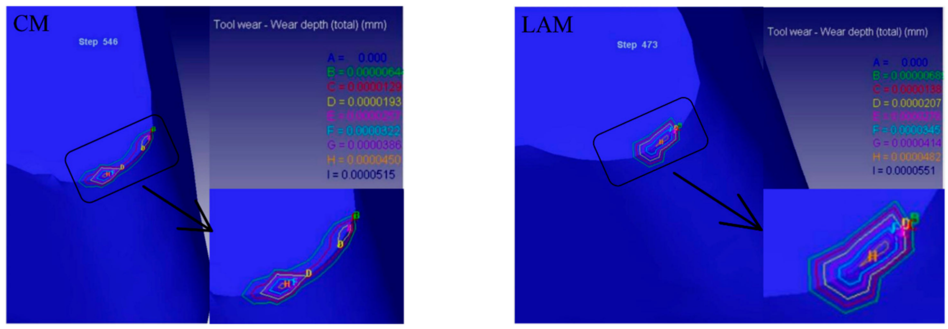

(**a**) (**b**)

Figure 6. The wear depth of the rake face at v_c = 50 m/min, f = 0.10 mm/r and ap = 0.5 mm: (**a**) conventional machining; (**b**) laser-assisted machining.

Table 5. Comparison of tool wear depths.

Test Group Number	CM Tool Wear Depth (nm)	LAM Tool Wear Depth (nm)	Difference (nm)	Percentage Share
001	72.5	75.3	−2.8	−3.86%
002	45	38.8	6.2	13.78%
003	65.8	47.7	18.1	27.51%
004	52	55.8	−3.8	−7.31%
005	62.8	50.1	12.7	20.22%
006	56.2	43.3	12.9	22.95%
007	47.1	48.2	−1.1	−2.34%
008	59.5	50.6	8.9	14.96%
009	50.7	42.7	8	15.78%

Table 6. Tool wear depth difference analysis.

Test Group Number	Cutting Speed v_c (m/min)	Cutting Depth a_p (mm)	Feeding Speed f (mm/r)
Kj1	−4.5%	12.48%	11.35%
Kj2	16.32%	11.95%	15.51%
Kj3	22.08%	9.47%	4.08%
Rj	26.58%	3.01%	11.43%
Primary and secondary levels		v_c, f and ap	
Optimum combination		v_3, ap1 and f_2	

Figure 7 shows the morphologies of flank wear surfaces via CM and LAM. Figure 8 shows that the maximum width of the flank wear via LAM was reduced by ~29% compared to that via CM, indicating that LAM can improve machining conditions, reduce flank wear and enhance the tool life. In addition, the hard spot wear and diffusion wear on the flank face via LAM were slightly more severe than with CM, because the cutting temperature of LAM was slightly higher than that of CM; as the cutting temperature increased, the workpiece material had a weaker tendency for work hardening, the friction factor between the chip and the tool surface decreased, and the maximum height of the built-up edges Hb decreased. Thus, the built-up edges fell off more frequently, generating more fragments, and the flank face had more grooves cut into it. In addition, because of the high cutting temperature, the chemical elements in the tool were more active, the diffusion rate was fast, and the degree of diffusion wear was more extreme.

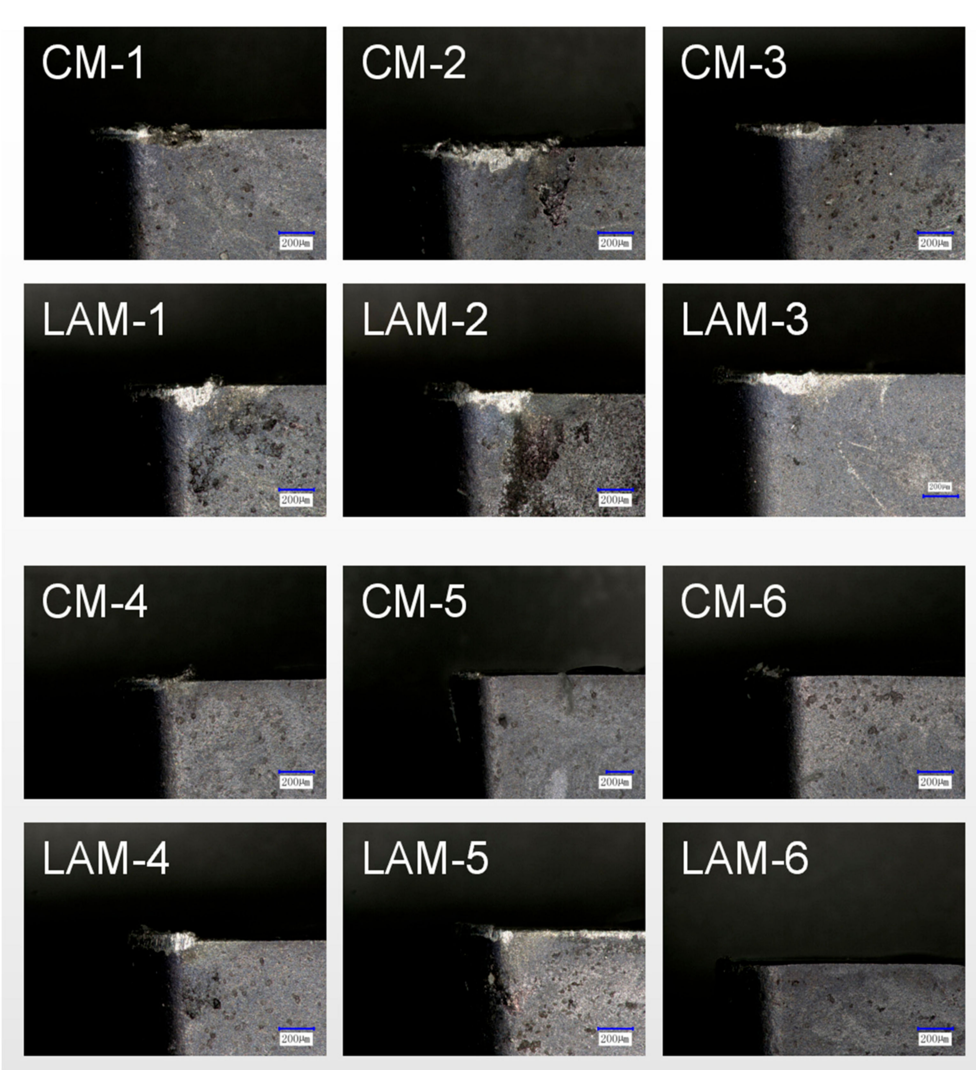

Figure 7. Comparison of flank wear morphologies via conventional machining and laser-assisted machining.

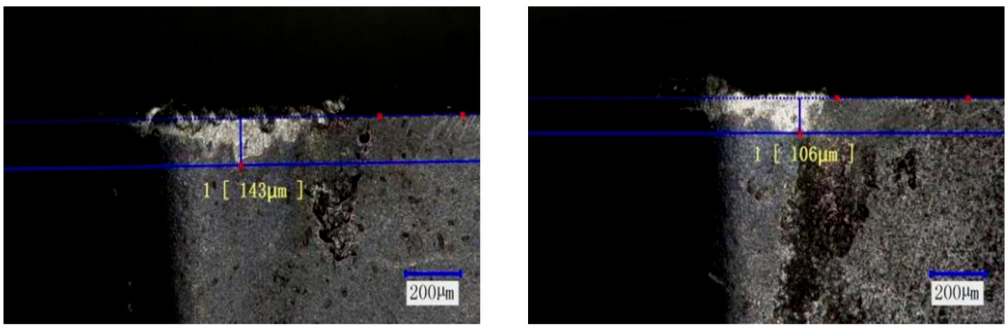

(**a**) (**b**)

Figure 8. The VBmax value in both conventional machining and laser-assisted machining (v_c = 50 m/min, f = 0.10 mm/rev and ap = 0.5 mm): (**a**) CM-2; (**b**) LAM-2.

3.3. Surface Roughness Analysis

Surface roughness is an essential parameter for evaluating the surface quality of a workpiece. It has a significant impact on the serviceability of the part, affecting not only the wear resistance and fatigue strength regions of the part, but also the contact stiffness and corrosion resistance [27]. As shown in Figure 9, the roughness of laser heating-assisted cutting was generally smaller than that of CM, and the least obvious one occurred in the second group. This is because when the cutting temperature reached 600°C, the chemical activity of titanium increased, and the chip reacted strongly with carbon monoxide, carbon dioxide and other gases in the air, resulting in embrittleness, loss of plasticity and reduced chip deformation and shrinkage ability. In addition, at high temperatures, the alpha phase in the alpha + beta titanium alloy shifted to a larger volume of the beta direction, causing the chip to grow, which resulted in the chip not being easily broken, the phenomenon of the tangled tool. This resulted in a secondary scratch of the machined surface during the machining process, which increased the surface roughness. Figure 10 depicts the cutting process. The most significant improvement in surface roughness occurred in group 7, with a reduction of approximately ~45.0%, for the following three main reasons.

First, because the nose- or wedge-shaped hard blocks formed by the growth and shedding of chip formers were smaller than conventionally machined hard blocks, the overcut ΔhD generated by the chip formers during the cutting process was small, resulting in shallow furrows carved in the direction of the cutting speed and the low roughness of the machined surface.

Second, under the same processing parameters, as the cutting temperature of LAM increased, it influenced the growth of the built-up edges during cutting, so that the maximum built-up edge height Hb was lower than that of CM. The detachment cycle of the top of the built-up edges was shorter; hence, pieces of built-up edges falling off and embedded in the machined surface were smaller than those with CM. The working rake angle of the tool changed in a small range during processing; therefore, the cutting force fluctuation range of the LAM was smaller than that of CM as shown in Figure 4b, leading to a tool vibration of the LAM, which was smaller than that of CM, and the vibrating tool pattern produced on the machined surface was lighter.

Third, during LAM, the cutting-edge wears and the microchipping of the tool were less than that of CM. In addition, as the yield strength of the workpiece decreased because of laser heating, the external force required to produce plastic deformation decreased, as does the plasticity of the material being machined, preventing the formation of scales.

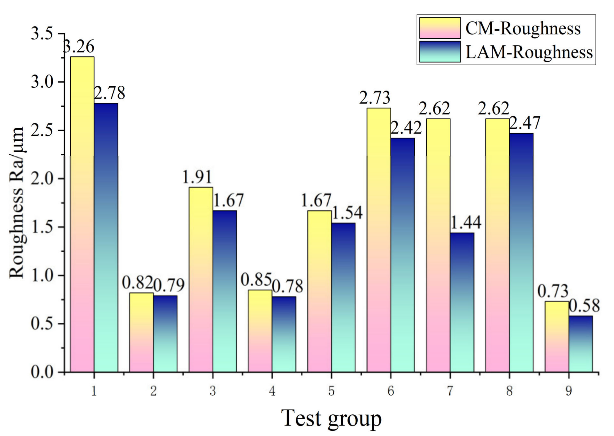

Figure 9. Comparison of surface roughness of the machined material via conventional machining and laser-assisted machining.

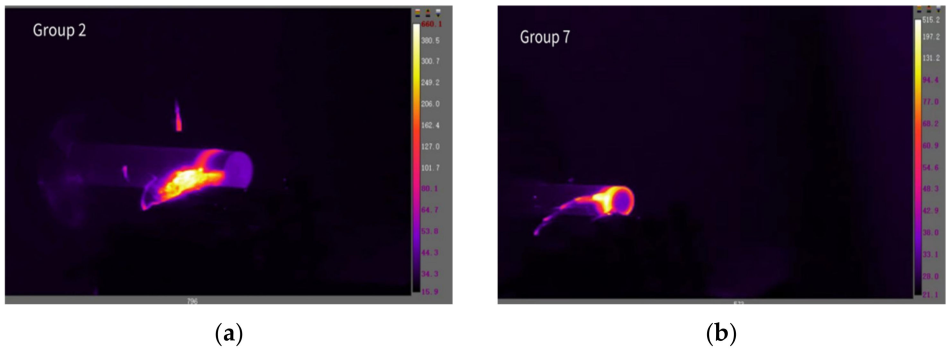

Figure 10. Temperature field nephogram of cutting process: (**a**) group II cutting process; (**b**) group VII cutting process.

The data obtained from the orthogonal tests of LAM were regressed to establish a correlation between surface roughness values and cutting parameters to guide production. SPSS software was used to conduct a linear regression analysis. The regression equation for the roughness values was assumed to be as follows [28]:

$$Ra = a_0 + a_1 \times v + a_2 \times f + a_3 \times a_p. \quad (6)$$

Table 7 displays the coefficients of the cutting parameters obtained after fitting, where $a_0 = -1.477$, $a_1 = 0.003$, $a_2 = 18.400$ and $a_3 = 0.625$. Therefore, the resulting multi-factor linear regression equation for surface roughness was as follows:

$$Ra = -1.477 + 0.003 \times v + 18.400 \times f + 0.625 \times a_p. \quad (7)$$

From the regression Equation (7), $|a3| > |a2| > |a1|$, according to the size of the regression parameters, the influences of degree of cutting parameters on the surface roughness can be judged from high to low were the cutting depth, the feed rate and the cutting speed. Furthermore, the surface roughness of CM of each cutting amount influenced degree size in the order of the feed > the cutting speed > the depth of cut [18].

This is caused by the different cutting speeds and feeds under the different heating layer depths, as shown in Figure 11. For the same laser parameters and a cutting speed of 70 m/min, the heated layer temperature and the depth were 400 °C and 0.105 mm, respectively. Moreover, for cutting speeds of 50 and 30 m/min, the heating layer depths were 0.181 and 0.259 mm, respectively. As the cutting speed increased, the depth of the heated layer of the workpiece decreased. Additionally, the surface area of the heat-affected zone created by the laser on the workpiece decreased.

Wang [24] found that the metallographic organisation of the surface layer of the workpiece at a certain depth would be altered after laser heating by irradiating the surface of titanium alloy with different laser parameters, resulting in the formation of three new phases. As shown in Figure 12, the hardness would exceed the original metallographic phase. The dendritic grain layer is the most superficial layer of the workpiece, followed by the needle grain layer. The transition layer of needle-like equiaxial grain is affected by the laser heating area to the normal metallographic transition area, its metallographic structure for the mixed distribution of needle-like grain and equiaxial grain and the bottom layer, which is primitive metallographic with equiaxed grain distribution.

It is evident that if the cutting depth was less than the depth of the laser processing metamorphic layer, there was a new metallic phase on the workpiece surface due to heating, increasing the degree of work hardening of the surface layer of the workpiece. This enhanced the deformation resistance, so that when the machined surface was completely out of contact with the flank face to produce an increase in the elastic force that caused its elasticity to recover. Therefore, the thin layer left by the machined layer could not be completely recovered, thus increasing the surface roughness. When the temperature was high, the alpha phase in the workpiece entered the beta phase, which increased the volume of the β phase. After the laser finished heating the workpiece, it was rapidly cooled and most of the alpha phase precipitated from the beta phase, forming a secondary alpha phase, which formed a strip-like sheet structure. The primary alpha and residual beta phases together formed the machined surface; however, due to the different grain sizes of the three phases, the machined surface was uneven, which eventually increased the surface roughness. Therefore, the depth of cut significantly affected the surface roughness of LAM of titanium alloys.

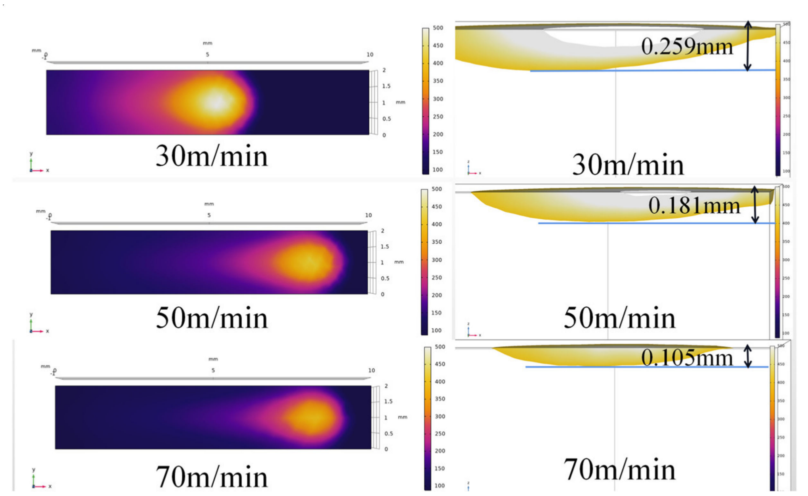

Figure 11. Depths of the heating layer at different cutting speeds.

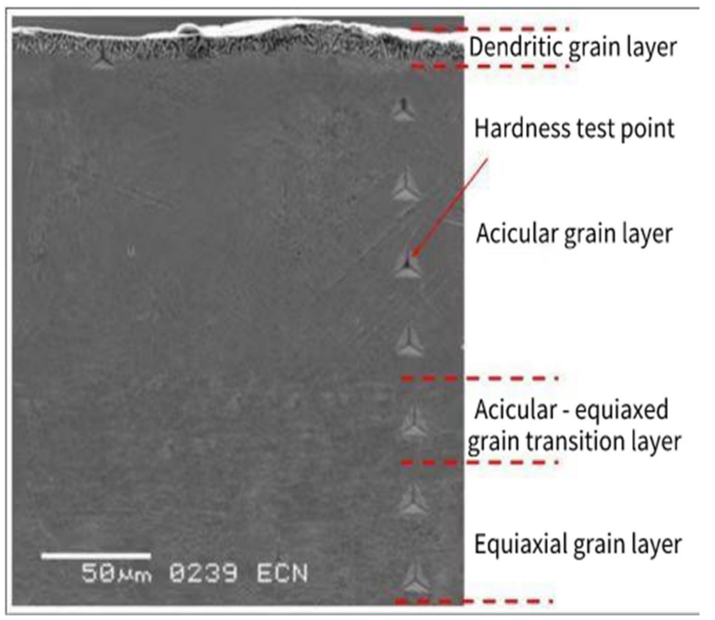

Figure 12. Metallographic organisation changes [24].

Table 7. Regression analysis coefficients of surface roughness [29].

Parameter	B	e	Bate	T	Sig.
Constant	−1.477	0.143		−10.317	0.000
Cutting speed	0.003	0.002	0.059	1.637	0.163
Feed rate	18.400	0.672	0.986	27.386	0.000
Cutting depth	0.625	0.168	0.134	3.721	0.014

Tables 8 and 9 show the extent to which the multi-factor linear regression equation fitted the test data. Table 8 shows a high R-value of 0.997, indicating a high correlation between the cutting parameters and the surface roughness values. The table also shows that the Durbin–Watson (D–W) value was 1.530, indicating that the residuals were independent and that the fitted equations were valid. The ANOVA is shown in Table 9, which shows a significance of 0.0001. Therefore, the fitted equation had a confidence level of 99.99%.

Table 8. Model summary.

R	R2	Adjusted R2	Standard Estimation Error	D–W Value
0.997	0.994	0.990	0.082	1.530

Table 9. ANOVA for surface roughness.

	Sum of Squares	Freedom	Mean Square	F	Sig.
Returning	5.190	3	1.730	255.512	0.0001
Residual	0.034	5	0.007		
Total	5.224	8			

The fitted equations from the regression analysis were used to test the test parameters. Table 10 shows that the relative errors of the eight groups were all within 10%, except for group 9. Hence, the fitted equations from the regression analysis were close to the actual values for the surface roughness of the workpiece and could predict the surface roughness of the workpiece after laser-assisted turning based on the cutting parameters.

The test parameters were examined using the fitted equation from the regression analysis. Table 10 shows that the maximum residual was 0.1125. Therefore, the fitted equation from the regression analysis was close to the actual value of the surface roughness of the workpiece and can predict the surface roughness of the workpiece after laser-assisted turning based on the cutting parameters.

Table 10. Surface roughness predictive analysis.

Observation Group	Measured Value	Predicted Value	Absolute Error	Relative Error
1	2.781	2.7255	0.0555	2.00%
2	0.793	0.8255	0.0325	4.10%
3	1.674	1.6855	0.0115	0.69%
4	0.782	0.7605	0.0215	2.75%
5	1.542	1.6205	0.0830	5.38%
6	2.423	2.4805	0.0575	2.37%
7	1.443	1.5555	0.1125	7.80%
8	2.474	2.4155	0.0585	2.36%
9	0.581	0.5155	0.0655	11.27%

4. Conclusions

This study used the finite element software DEFORM-3D to develop a predictive model for conventional turning and laser-assisted turning of the titanium alloy TC6 in three dimensions. Furthermore, the theoretical study of the LAM of TC6 titanium alloy has been further improved to provide a theoretical reference for industrial applications of LAM of titanium alloy. The following conclusions were drawn:

(1) When the cutting speed exceeded 50 m/min, the depth of wear on the rake face of the tool ias more significant than that obtained via CM due to insufficient laser heating, and the yield strength of the cutting layer material was reduced less. Instead,

the cutting temperature was higher in the case of laser heating than CM. When compared to CM, LAM at a cutting speed of less than or equal to 50 m/min reduced the maximum width of the rear tool face wear by approximately ~29%.

(2) The laser heated surface temperature exceeded 600 °C, making it easy for chips to become entangled in the machining process and thus resulting in poor roughness improvement.

(3) Because of the depth of the laser-heated layer and the thermal change in the metallographic structure, the cutting depth of laser heating-assisted cutting on surface roughness of the significant degree of influence, cutting processing should make the cutting depth larger than the thickness of the laser heating metamorphic layer. Otherwise, it will exacerbate the hardening of the machined surface.

(4) Using extreme difference analysis, the best combination of cutting parameters for tool wear improvement were v_c = 30 m/min, f = 0.15 mm/r and a_p = 0.5 mm. The roughness prediction equation was obtained using regression analysis as given in Equation (7).

Author Contributions: Conceptualisation, X.K. and X.L.; methodology, N.H. and X.K.; software, Z.D.; validation, M.W. and X.L.; formal analysis, Z.D.; investigation, Z.D.; resources, N.H.; data curation, M.W.; writing—original draft preparation, Z.D.; writing—review and editing, M.W. and X.K.; visualisation, N.H.; supervision, X.L.; project administration, X.L. and N.H.; funding acquisition, X.K. All authors have read and agreed to the published version of the manuscript.

Funding: This research was supported by the Aviation fund (No.2019ZE054005), Natural Science Foundation of Liaoning Province (2021-MS-264), Project planned by Shenyang Science and Technology Bureau (RC210439) and Education Department of Liaoning Province Project (No. JYT2020058).

Informed Consent Statement: Informed consent was obtained from all subjects involved in the study.

Data Availability Statement: Not applicable.

Acknowledgments: The authors gratefully acknowledge the financial support from the Aviation fund (No.2019ZE054005), Natural Science Foundation of Liaoning Province (2021-MS-264), Project planned by Shenyang Science and Technology Bureau (RC210439) and Education Department of Liaoning Province Project (No. JYT2020058).

Conflicts of Interest: The authors declare that they have no known competing financial interests or personal relationships that could have appeared to influence the work reported in this paper.

Abbreviations

CM	conventional machining
LAM	laser-assisted machining
Rm	tensile strength
v_c	cutting speed
ap	cutting depth
f	feeding speed
Q	the surface heat flux of the laser irradiation region
r0	the radius of the laser spot
α	the absorption rate of laser energy of the heated material
P	the laser power
r	the distance from a point to the center of the laser spot
σ	the yield limit
ε_i	the equivalent plastic strain
$\dot{\varepsilon}$	the equivalent plastic strain rate
$\dot{\varepsilon}_0$	the initial strain rate
A	the initial yield stress of the material
B	the hardening coefficient

C	the strain rate coefficient
m	the temperature softening coefficient
n	the work hardening coefficient
T	the deformation temperature
T_r	the room temperature (20 °C)
T_m	the melting point of the material
τ_f	the frictional shear stress
σ_n	the positive stress
τ_p	the shear strength
μ	the coefficient of friction
ω	the wear depth
dt	the change in time
p	the interface pressure
v	the sliding speed
T	the absolute interface temperature
Δh_D	Amount of over cutting
H_b	the maximum built-up edges height
D–W	Durbin–Watson

References

1. Ezugwu, E.O. Key improvements in the machining of difficult-to-cut aerospace superalloys. *Int. J. Mach. Tool. Manuf. Des. Res. Appl.* **2005**, *45*, 1353–1367. [CrossRef]
2. Tiantian, L.I.; Zhanqiang, L.; Xiaoqin, W. Study on cutting performance of titanium alloy for high-speed cutting of PCBN tools. *Tool. Technol.* **2008**, *42*, 24–27. [CrossRef]
3. Haoqian, M.; Dong, Y.; Donghua, C.; Kanghui, W. Abaqus-based cutting simulation and process optimization of titanium alloy Ti_6Al_4V. *Manuf. Autom.* **2020**, *42*, 23–27. [CrossRef]
4. Yuyan, N.; Liang, W.; Jilin, Z.; Xiaojun, L.; Xiangbin, Y. Study on material properties of Cemented Carbide Tool Milling Ti_6Al_4V. *Mach. Manuf.* **2022**, *60*, 39–42. [CrossRef]
5. Zhangyong, J.C.; Yingying, Z. Study on the effect of cutting parameters on the cutting force of turning titanium alloy. *Tool. Technol.* **2021**, *55*, 23–27.
6. Zhenghuan, W.; Chaofeng, Z. Research on cutting force prediction during titanium alloy milling based on multilayer fusion network. *Manuf. Technol. Mach. Tool.* **2022**, *9*, 90–96. [CrossRef]
7. Ding, Y.; Xuefeng, W.; Yanchao, G.; Shuiwang, W.; Mingjun, C.; Lijun, Y. Research review on laser composite removal processing technology. *Aerosp. Manuf. Technol.* **2022**, *65*, 30–47. [CrossRef]
8. Rudranarayana, K.; Susanta, S.; Ananda, S. Ultrasonic vibration-assisted turning of Titanium alloy Ti-6Al-4V: Numerical and experimental investigations. *J. Braz. Soc. Mech. Sci. Eng.* **2020**, *42*, 399. [CrossRef]
9. Rui, W.; Xiaoqing, Z.; Tijie, S.; Yi, Z. TA15 titanium alloy laser cutting heat affected zone microstructure and properties research. *J. Hot Work. Process.* **2018**, *47*, 75–78.
10. Ginta, T.L.; Amin, A.K.M.; Lajis, M.A. Suppressed Vibrations During Thermal-assisted Machining of Titanium Alloy Ti-6Al-4V using PCD Inserts. *J. Appl. Sci.* **2012**, *12*, 2418–2423. [CrossRef]
11. Habrat, W.F. Experimental Investigation of Effect of the Laser-Assisted Finish Turning of Ti-6Al-4V Alloy on Machinability Indicators. *Solid State Phenom.* **2017**, *4550*, 135–142. [CrossRef]
12. Woo, W.-S.; Kim, E.-J.; Jeong, H.-I. Laser-Assisted Machining of Ti-6Al-4V Fabricated by DED Additive Manufacturing. *Int. J. Precis. Eng. Manuf.-Green Technol.* **2020**, *7*, 559–572. [CrossRef]
13. Yanfeng, G.; Jianhua, X. Tool Wear Characteristics of Ti-6Al-4V Alloy in Laser-Assisted Milling. *China Mech. Eng.* **2016**, *27*, 2877–2883.
14. Kalantari, O.; Jafarian, F.; Fallah, M.M. Comparative investigation of surface integrity in laser assisted and conventional machining of Ti-6Al-4 V alloy. *J. Manuf. Process.* **2021**, *62*, 90–98. [CrossRef]
15. Ayed, Y.; Germain, G.; Salem, W.B.; Hamdi, H. Experimental and numerical study of laser-assisted machining of Ti_6Al_4V titanium alloy. *Finite Elem. Anal. Des.* **2014**, *92*, 72–79. [CrossRef]
16. Kim, D.-H.; Lee, C.-M. Experimental Investigation on Machinability of Titanium Alloy by Laser-Assisted End Milling. *Metals* **2021**, *11*, 1552. [CrossRef]
17. Dandekar, C.R.; Shin, Y.C.; Barnes, J. Machinability improvement of titanium alloy (Ti–6Al–4V) via LAM and hybrid machining. *Int. J. Mach. Tools Manuf.* **2010**, *50*, 174–182. [CrossRef]
18. Xianjun, K.; Guang, H.; Biao, L.; Zhi, D.; Yanhai, C.; Minghai, W. Optimization analysis of cutting forces and surface roughness of titanium alloy turning. *Tool. Technol.* **2022**, *56*, 20–25. [CrossRef]
19. Yang, B.; Lei, S. Laser-Assisted Milling of silicon nitride ceramic: A machinability study. *Int. J. Mechatron. Manuf. Syst.* **2008**, *1*, 116–130. [CrossRef]

20. Zheng, Z. Study on Laser Assisted Micro-Milling of TC4 Titanium Alloy. Master's Thesis, Harbin Institute of Technology, Harbin, China, 2014.
21. Xu, Y.; Cheng, L.; Shu, C.; Peiyuan, L. Foreign Object Damage Performance and Constitutive Modeling of Titanium Alloy Blade. *Int. J. Aerosp. Eng.* **2020**, *2020*, 2739131. [CrossRef]
22. Xiao, Z.; Wuyin, J. Finite Element Simulation of Titanium Alloy High Speed Turning Based on DEFORM3D. *Tool. Tech.* **2017**, *51*, 45–48.
23. Park, Z. Key technologies and scientific issues in laser assisted cutting. *Sci. Technol. Eng.* **2016**, *21*, 140–149.
24. Lihao, W. Simulation analysis and experimental study of laser assisted turning process of titanium alloy Ti_6Al_4V. Master's Thesis, Harbin Institute of Technology, Harbin, China, 2016. [CrossRef]
25. Shuyi, X.; Shihong, W. *Aluminum Alloy and Titanium Alloy*; China Machine Press: Beijing, China, 1987.
26. Zaiwei, L.; Lin, B.; Xiaohu, L.; Anyao, D. Study on the effect of laser-assisted machining on tool wear based on molecular dynamics simulation. *Diam. Relat. Mater.* **2020**, *109*, 108022. [CrossRef]
27. Hongxing, T. Analysis of influencing factors of machining surface quality and improvement measures. *Sci. Technol. Enterpr.* **2015**, *37*, 213. [CrossRef]
28. Xiaoyu, N. Laser Assisted Microturning Test and Surface Influence Law of TB8 Titanium Alloy. Master's Thesis, Changchun University of Science and Technology, Changchun, China, 2021. [CrossRef]
29. Przestacki, D.; Jankowiak, M. Surface roughness analysis after laser assisted machining of hard to cut materials. *J. Phys. Conf.* **2014**, *483*, 12–19. [CrossRef]